Pressure-induced transformations in Ce-Al metallic glasses: the role of stiffness of interatomic pairs

P. Dziegielewski[a], J. Antonowicz[a,*], A. Pietnoczka[a], O. Mathon[b], S. Pascarelli[b], I. Kantor[c], T. Shinmei[d], T. Irifune[d]

[a] *Faculty of Physics, Warsaw University of Technology, Koszykowa 75, 00-662 Warsaw, Poland*
[b] *European Synchrotron Radiation Facility, F-38043 Grenoble, France*
[c] *Technical University of Denmark, Fysikvej 307, 2800 Kgs. Lyngby, Denmark*
[d] *Geodynamics Research Center, Ehime University, 2-5 Bunkyo-cho, Matsuyama 790-8577, Japan*

Abstract

When high pressure is applied to Ce-Al metallic glasses, their disordered atomic structure exhibits some unusual properties like polyamorphism or transformation into a crystalline phase. In this work we probe the local environment of cerium in $Ce_{55}Al_{45}$ and $Ce_{75}Al_{25}$ glasses by X-ray absorption spectroscopy and X-ray diffraction in the pressure range of 0-30 GPa. Due to compositional dependence of stiffness of Ce-Al pairs, densification of $Ce_{55}Al_{45}$ is accompanied by an increase of atomic size mismatch between Ce and Al stabilizing the amorphous phase, while a decrease of the mismatch is observed in $Ce_{75}Al_{25}$ alloy which eventually leads to its devitrification.

Keywords: extended X-ray absorption fine structure (EXAFS), metallic glass, crystallization, high pressure

Due to its unique electronic configuration, cerium metal is known to exhibit a complex pressure-temperature phase diagram involving a number of allotropic crystalline phases [1]. This phase variety is attributed to presence of a single $4f$ electron in the valence band of cerium which can vary its degree of localization with the external pressure. Cerium-based amorphous alloys (metallic glasses

*Corresponding author
Email address: jerzy.antonowicz@pw.edu.pl (J. Antonowicz)

- MGs) also possess some intriguing pressure-related properties. Sheng *et al.* [2] reported on „polyamorphism"- pressure-induced transition between two distinct amorphous polymorphs in $Ce_{55}Al_{45}$ MG. The transition was attributed to delocalization of $4f$-electrons and the resulting density change. More recently, $Ce_{75}Al_{25}$ MG was found to undergo an unexpected transformation into a cubic single crystal at pressure of 25 GPa as a result of collapse of Ce atoms [3]. Subsequent research on Ce-based MGs revealed more details of the polyamorphic transition and pressure-induced devitrification (PID) providing experimental evidence of $4f$ electron delocalization [4], split in Ce-Ce nearest neighbours shell [5] and link between the polyamorphism and phase transformation between γ-Ce and α-Ce [6, 7]. Recently, the role of Ce $4f$ electron delocalization in PID has been questioned and the crystallization has been explained in terms of Bader volume [8]. In their initial report on PID in $Ce_{75}Al_{25}$ Zeng et al. attributed the glass-crystal transition to presence of hidden long-range fcc topological order in metallic glasses [3]. Same authors have demonstrated [9] that PID occurs in a narrow composition range which can be explained by a semi-empirical topological instability criterion proposed by Egami [10] and based on atomic size mismatch. In this interpretation, the atomic size difference between Ce and Al is significantly reduced by pressure so the actual solute content becomes smaller than a critical value necessary for destabilization of the crystal solid solution.

In this work, we exploit extended X-ray absorption fine structure (EXAFS) and X-ray diffraction (XRD) to probe atomic arrangement of $Ce_{55}Al_{45}$ and $Ce_{75}Al_{25}$ melt-quenched glassy ribbons in high hydrostatic pressure condition. By following the pressure dependence of parameters of short-range order around cerium we demonstrate that the stiffness of Ce-Al interatomic interactions strongly varies with alloy composition. As a result, the applied hydrostatic pressure can either increase or decrease the effective size mismatch between Ce and Al atoms. Depending on the variation of the atomic mismatch with pressure, the structurally disordered glass can be either further stabilized in its metastable state or can transform into an ordered crystalline phase.

The ingots of $Ce_{55}Al_{45}$ and $Ce_{75}Al_{25}$ alloys (composition given in at. %)

were prepared from 99.9% purity elements in an arc-melter applying multiple remelting to ensure homogeneity. The glassy samples were obtained by rapid quenching using a melt-spinning set-up operating under argon atmosphere and applying wheel speed of about 30 m/s. The resulting ribbons were stored in silicon oil protecting them from oxidation. High-pressure X-ray absorption measurement was carried out using a mechanical piston-cylinder diamond anvil cell [11]. To avoid unwanted signal distortions of EXAFS spectra we used recently developed sintered nano-polycrystalline diamond (NPD) anvils [12] which provide clean glitch-free EXAFS spectra in any energy range [13]. The EXAFS experiment at Ce K-edge (40443 eV) was carried out in transmission mode at BM23 beamline of the European Synchrotron Radiation Facility. Supplementary X-ray diffraction (XRD) patterns were collected at the X-ray beam energy of 40 keV using a 2D CCD detector. To optimize sample thickness for the absorption experiment the ribbons were polished down from their initial thickness of $\sim$40 μm down to 15 μm. The thinned ribbons were subsequently cut into $\sim$50 $\times$50 μm pieces and loaded into NPD anvil cell using ethanol-methanol mixture as a pressure-transmitting medium. During the synchrotron experiment the pressure was changed manually in the range of 0-30 GPa and its value was monitored by measuring fluorescence from small chips of ruby placed inside the pressure cell. For additional pressure determination, small pieces of gold foil were placed next to the sample and diffraction patterns of gold were recorded. The X-ray beam was focused down to $\sim$5 $\times$5 μm and two miniature ion chambers were used to measure the incoming and transmitted X-ray flux. More details on the high-pressure EXAFS set-up at BM23 beamline are given elsewhere [14, 15].

Selected 2D XRD patterns of $Ce_{55}Al_{45}$ and $Ce_{75}Al_{25}$ taken in the low and the high-pressure regime are shown in Figure 1a. Since most of the X-ray scattering comes from the anvils, the dominant feature of the patterns are strong continuous rings originating from nanocrystalline diamond. Superimposed on the NPD signal is a relatively weak amorphous "halo" pattern. The halo symmetrically expands with pressure which is a signature hydrostatic compression

of the sample. Apart from intense diamond rings, no traces of Bragg reflection from the crystalline phases are observed for $Ce_{55}Al_{45}$ up to 30 GPa. However, for $Ce_{75}Al_{25}$ the initially fully amorphous sample undergoes a partial transformation into a crystalline phase which is manifested by appearance of single, intense spots in the 2D images. Figure 1b presents azimuthally integrated XRD spectra of both investigated alloys for selected pressure values as plots of intensity vs. q ($q = 4\pi \sin\theta/\lambda$ where θ is half of the scattering angle and λ is the X-ray wavelength). The diffraction peaks appearing around 25 GPa were identified as Bragg reflections from cubic Ce_3Al intermetallic compound - a crystalline polymorph of $Ce_{75}Al_{25}$ glassy alloy. The critical pressure at which the devitrification takes place is in excellent agreement with previously reported values for the same alloy [3, 9]. We note that in our case we do not observe a complete transformation of the whole glassy sample into a monocrystal [3]. Given the fact that only single diffraction spots are visible in the XRD pattern and that both sample thickness and X-ray beam size are of the order of 10 μm, it is reasonable to assume that in our experiment we observe a single, micron-scale Ce_3Al crystal coexisting with an amorphous phase. The partial transformation can be possibly explained by sample inhomogeneity or defects which can arise from preparation of the specimen.

The current XRD results support the previously reported PID occurring in $Ce_{75}Al_{25}$ MG but also allow estimation of the elastic properties of the investigated Ce-Al MGs. The observed expansion of the amorphous halo reflects the decrease of the mean atom spacing of the system which is inversely proportional to the position of the halo in the azimuthally integrated spectrum. Since volume of the system scales with mean atom spacing cubed, one can relate the volume change with the q-position of halo maximum – q_m. The relationship between the volume change and the applied pressure can be described in terms of isothermal equation of state (EOS) involving bulk modulus K, which is the measure of materials resistance to compression. Here, we have employed second-order Birch-Murnaghan EOS [16] $P(V) = 3K/2[(V_0/V)^{7/3} - (V_0/V)^{5/3}]$ replacing $(V_0/V)^{1/3}$ with (q_m/q_{m0}) where q_{m0} refers to value at zero pressure. The re-

sults of EOS fitting to the XRD data measured during compression are shown in Figure 1c. The fitting yields $K = 26(3)$ GPa and $K = 34(2)$ for $Ce_{55}Al_{45}$ and $Ce_{75}Al_{25}$ respectively. The obtained values of K are close to those reported previously for Ce-based MGs [7]. We note that the narrow hysteresis for $Ce_{55}Al_{45}$ visible in Figure 1c up to ~ 15 GPa is a signature of polyamorphism and is in good agreement with previous reports for the same alloy composition [2].

It was demonstrated by Wang[17] that MGs inherit their elastic properties from their solute (base) atoms and the overall stiffness of the MG is determined by the weakest solvent-solvent bonds. This tendency has been confirmed in our recent high-pressure EXAFS work where we found that the bulk modulus of Zr-based MG is controlled by the stiffness of Zr-Zr pairs [15]. Since bulk modulus of crystalline cerium metal is over three times smaller than that of crystalline aluminium ($K_{Ce} = 22$ GPa and $K_{Al} = 76$ GPa), one should expect that compressibility of Ce-Al MG increases with increasing Ce content since it gets dominated by soft Ce-Ce pairs. Surprisingly, the values of bulk modulus derived from XRD data point to an opposite trend. This non-trivial compositional dependence of the elastic properties can be understood when stiffness of different atomic pairs is examined in more detail.

To gain insight into the atomic-level mechanism of deformation of Ce-Al MGs we carried out a quantitative analysis of Ce K-edge high-pressure EXAFS data. Figures 2a-d present selected χ functions (χ is the EXAFS function) plotted as oscillations in k-space (k is a photo-electron wavenumber) and as a function of radial distance R (magnitude of Fourier-transformed $\chi(k)$). Two main trends in evolution of EXAFS spectra can be immediately observed in Figures 2b and 2d: a shift of the main maximum of $\chi(R)$ towards lower distances and an increase of its intensity. The shift is a signature of shortening of the interatomic distances resulting from increasing external pressure and the rise of the peak intensity results from progressive increase of the short-range order (more narrow distribution of interatomic distances) around cerium. The EXAFS fitting procedure consisted of two stages. In the first stage, for each EXAFS spectrum the fitting procedure yielded five numbers: two values of interatomic distances R_{Ce-Ce} and

R_{Ce-Al}, two values of mean-square relative displacement in the interatomic distance (Debye-Waller factors) σ^2_{Ce-Ce} and σ^2_{Ce-Al}, and the ratio between the number of Ce and Al nearest neighbours of Ce N_{Ce-Ce}/N_{Ce-Al}. The absolute values of Ce partial coordination numbers were evaluated under the arbitrary assumption that the total coordination of Ce is equal to 14. We underline that this assumption does not affect the main conclusions of the present study since it can contribute only to a small (few percent) systematic error of σ^2. In the course of fitting, we found that N_{Ce-Ce}/N_{Ce-Al} does not vary systematically over pressure and roughly scales with alloy composition. To limit the overall number of the independent fitting parameters and thus reduce the uncertainty of estimation of R and σ^2, in the final stage of EXAFS fitting we kept the values of partial coordination number constant and equal to a product of the total coordination number of cerium (14) and the atomic content of a given element. Namely, we fixed partial coordination numbers as $N_{Ce-Ce} = 10.5$, $N_{Ce-Al} = 3.5$ for $Ce_{75}Al_{25}$ and $N_{Ce-Ce} = 7.7$, $N_{Ce-Al} = 6.3$ for $Ce_{55}Al_{45}$. It should be mentioned that all EXAFS spectra in the pressure range up to 30 GPa were taken into account in our analysis, including the last two data points (25.3 GPa and 30.3 GPa) measured on the partly crystallized $Ce_{75}Al_{25}$ (see Figure 1b), by assuming the presence of a relatively low crystalline volume fraction.

The evolution of interatomic pair distances R and Debye-Waller factors σ^2 resulting from EXAFS fitting is presented in Figures 2e-f. As expected, both Ce-Ce and Ce-Al interatomic distances become shorter as pressure increases. The vales of the interatomic distances extrapolated to zero pressure reasonably coincides with the sum of Goldschmidt radii of the involved elements (r_{Al} =143 pm and r_{Ce}=182.5 pm): 3.65 Å for Ce-Ce and 3.26 Å for Ce-Al. From Figure 2f and Figure 2h it is apparent that while the values of σ^2 for Ce-Ce and Ce-Al are similar in $Ce_{55}Al_{45}$, in $Ce_{75}Al_{25}$ the disorder in Ce-Ce is significantly higher than that in Ce-Al pairs. Closer inspection of the pressure dependence of Ce-Ce and Ce-Al interatomic pair distances (Figures 2e and 2g) reveals the origin of the compositional dependence of the overall bulk modulus derived from XRD. The compressibility of specific pairs was quantified by EOS fitting to the

relative variation of interatomic distance substituting $(V_0/V)^{1/3}$ in the EOS with (R_0/R) where R_0 refers to zero pressure. As illustrated in Figure 3, the stiffness on Ce-Ce pairs varies only slightly between the two composition (49(4) GPa and 37(6) GPa for $Ce_{55}Al_{45}$ and $Ce_{75}Al_{25}$ respectively). However, the value of K for Ce-Al pairs considerably increases from 25(3) to 68(6) GPa when Al content varies between 45 and 25%. We argue that the difference of the overall bulk modulus of the two Ce-Al MG derived from the XRD results primarily from significantly more stiff Ce-Al interactions in $Ce_{75}Al_{25}$ as compared to $Ce_{55}Al_{45}$. In our interpretation, the composition-dependant stiffens of Ce-Ce and Ce-Al pairs not only controls the elastic properties of the two investigated glassy alloys but also underlies the PID in $Ce_{75}Al_{25}$. As suggested initially by Zeng et al. [9] the mechanism of the PID of Ce-Al MGs can be understood within the topological instability criterion proposed by Egami and Waseda [10]. According to this semi-empirical approach, for a binary solution the critical minimum solute concentration C_b^* required to destabilize the crystalline solid solution and form a glass is given by: $C_b^*|(r_b/r_a)^3) - 1| \approx 0.1$ where r_a and r_b are concentrations of solvent and solute atoms respectively. By analysing the effect of composition on PID in Ce-Al MGs Zeng et al. have found that PID occurs in a narrow composition range below the saturated critical value under high pressure and above the value required for glass formation at ambient pressure ($19\% < C_{Al} < 27\%$). The second condition for occurrence of PID proposed by Zeng is that larger atoms (Ce in this case) have to be more compressible than the small one (Al in this case). Authors of [9] argued that due to Ce-Al interactions the existing data on high-pressure radii of pure Ce and Al cannot be used. For this reason, in their predictions they have extracted the effective radii of Ce and Al in Ce-Al MG from molecular dynamics simulations and used those to derive the pressure dependence of the critical minimum solute concentration of Al.

We argue that due to strong composition dependence of elastic properties of Ce-Al interactions the overall physical picture of pressure-induced transformations in Ce-Al MGs is more complex, but still consistent with the topological

instability criterion. The values of effective atomic radius of Ce and Al can be readily calculated from the interatomic distances: $r_{Ce} = R_{Ce-Ce}/2$ and $r_{Al} = R_{Ce-Al} - R_{Ce-Ce}/2$. Since the stiffness of Ce-Al pairs increases significantly from $K = 25$ GPa to $K = 68$ GPa as Al content varies from 45 to 25%, the effective atomic volume mismatch exhibits different pressure dependences in the two investigated MGs. As demonstrated in Figure 4, at the equilibrium pressure P=0 GPa $(r_{Al}/r_{Ce})^3$ is similar in $Ce_{55}Al_{45}$ and $Ce_{75}Al_{25}$ MGs and equal to ~ 0.53. This number is consistent within the experimental error with the value of 0.48 calculated from Goldschmidt radii of Al and Ce. However, while the volume mismatch gets more pronounced in $Ce_{55}Al_{45}$ ($(r_{Al}/r_{Ce})^3$ deviates more from unity) it decreases in $Ce_{75}Al_{25}$ since the value of $(r_{Al}/r_{Ce})^3$ rises from ~ 0.53 to ~ 0.67 when going from 0 to 30 GPa. For both alloy compositions a critical volume mismatch required for topological instability of the glassy phase can be determined from the Egami criterion. The resulting values marked by the dashed lines in Figure 4 are approximate threshold values above which the amorphous phase becomes unstable against transformation into the crystalline state. Apparently, the threshold value of volume mismatch is reached only in the case of $Ce_{75}Al_{25}$, while for $Ce_{55}Al_{45}$ critical mismatch is never attained and thus PID does not occur. Due to a scatter of the data points and the approximate character of the Egami criterion, the critical value of pressure required for the PID is difficult to establish accurately. Nevertheless, judging from Figure 4 $Ce_{75}Al_{25}$ MG should crystallize at about 20 GPa, which is in fair agreement with the value of 25 GPa for which the PID is observed in diffraction. As a final remark, we note that in our EXAFS results we did not find any clear evidence of the polyamorphic transition in $Ce_{55}Al_{45}$ evidenced by the XRD. This can be explained by the fact that the density variation associated with polyamorphism is not detectable by a local probe such as EXAFS.

In conclusion, by combined high-pressure EXAFS and XRD analysis of the atomic order in $Ce_{55}Al_{45}$ and $Ce_{75}Al_{25}$ MGs we have demonstrated that the compositional dependence of stiffens of Ce-Al pairs underlies pressure-driven atomic rearrangements which for $Ce_{75}Al_{25}$ MG lead to its devitrification result-

ing from the topological instability of the amorphous phase.

Acknowledgments

We acknowledge the European Synchrotron Radiation Facility for provision of synchrotron radiation facilities. Professor A.R. Yavari is kindly acknowledged for his help with sample preparation and helpful conversations.

List of Figures

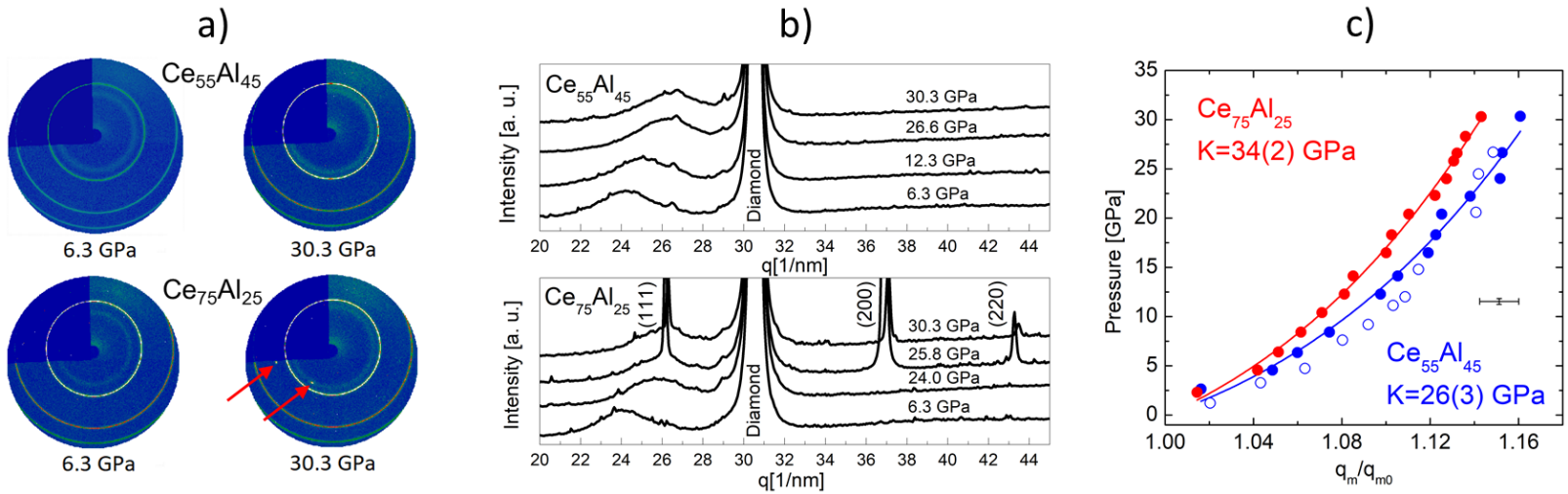

Figure 1: (a) Two-dimensional XRD patterns collected in transmission mode. Diffraction spots originating from crystalline Ce_3Al phase are indicated by arrows. (b) Azimuthally integrated intensity vs. q spectra. Peak indexes refer to cubic Ce_3Al. (c) Pressure dependence of the relative q-position of the amorphous halo. Full symbols indicate data points taken during increasing pressure ramp, open symbols represent decreasing pressure. Solid lines are EOS fits to the data points taken during compression. Cross indicates the error bars.

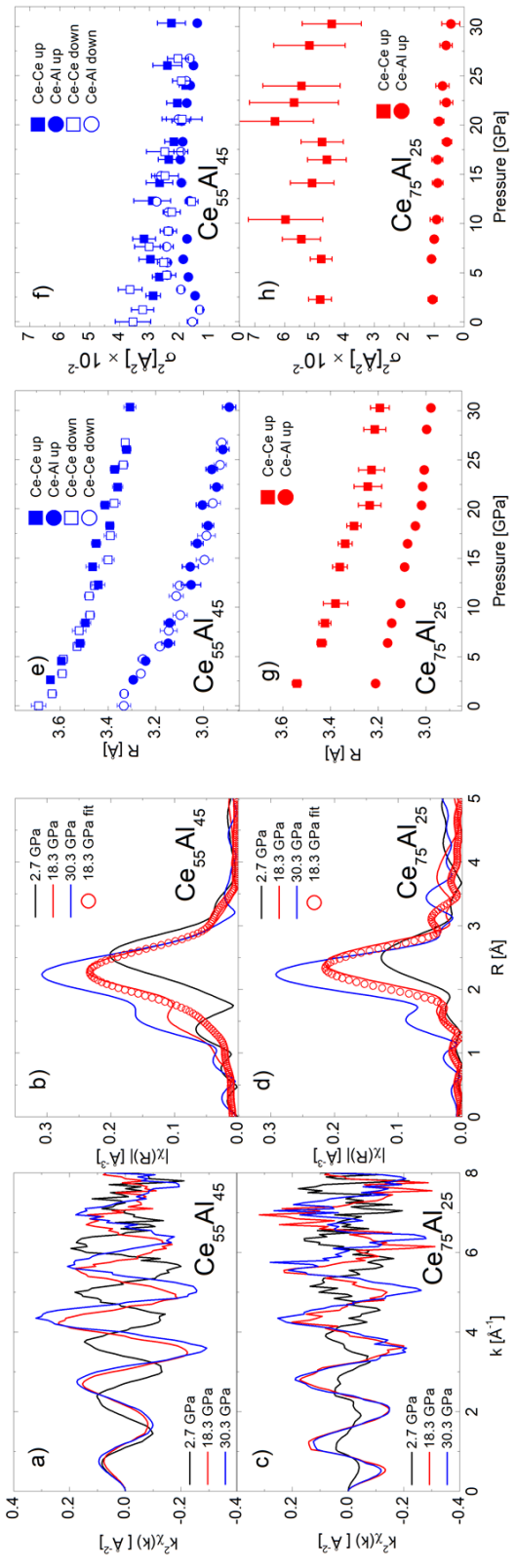

Figure 2: Selected Ce K-edge EXAFS spectra of $Ce_{55}Al_{45}$ and $Ce_{75}Al_{25}$ MGs plotted in k (a, c) and R (b, d) -space. Open symbols in (b) and (d) represent selected best fits in R-space. The results of EXAFS fitting: interatomic distances (e, f) and Debye-Waller factors (g, h). Full symbols indicate data points taken during increasing pressure ramp, open symbols represent decreasing pressure.

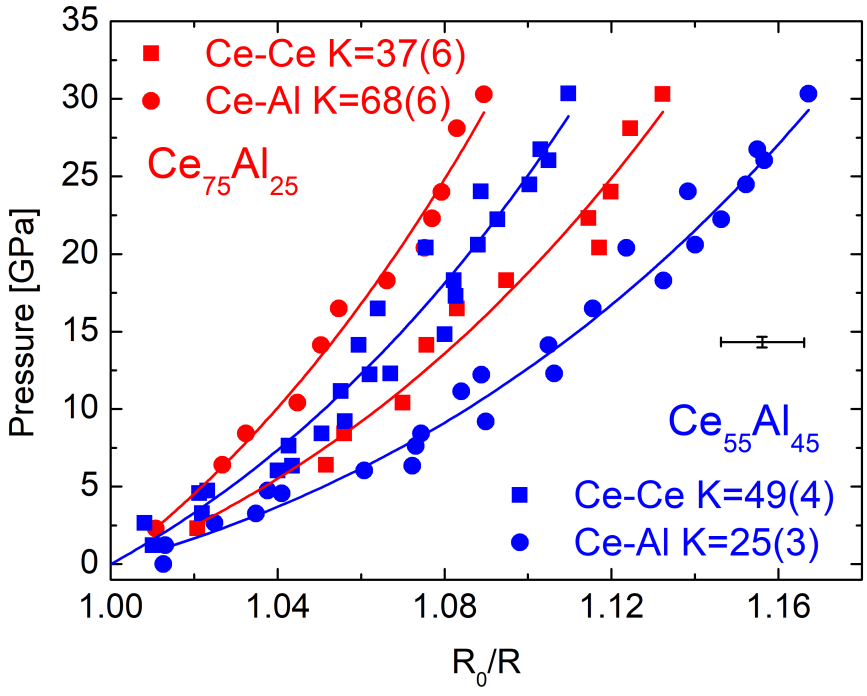

Figure 3: EOS fits to the relative variation of interatomic distances R_0/R derived from EXAFS (lines). Symbols represent data taken during both increasing and decreasing pressure ramp. Cross indicates the error bars.

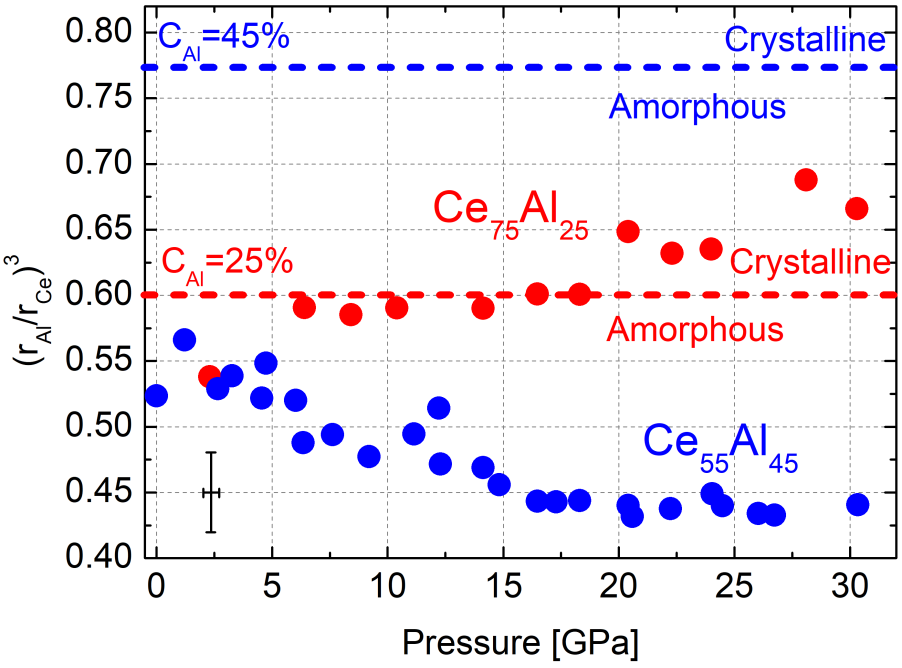

Figure 4: Relative atomic volume mismatch $(r_{Al}/r_{Ce})^3$ as a function of the applied pressure. The dashed lines indicate critical values of mismatch for Ce-Al alloys containing 45% (blue) and 25% (red) of aluminium. Symbols represent data taken during both increasing and decreasing pressure ramp. Cross indicates the error bars.

References

[1] B. Johansson, The α - γ transition in cerium is a mott transition, Phil. Mag. 30 (3) (1974) 469–482.

[2] H. W. Sheng, H. Z. Liu, Y. Q. Cheng, J. Wen, P. L. Lee, W. K. Luo, S. D. Shastri, E. Ma, Polyamorphism in a metallic glass, Nat. Mater. 6 (2007) 192.

[3] Q. Zeng, H. Sheng, Y. Ding, L. Wang, W. Yang, J.-Z. Jiang, W. L. Mao, H.-K. Mao, Long-range topological order in metallic glass, Science 332 (6036) (2011) 1404–1406.

[4] Q.-s. Zeng, Y. Ding, W. L. Mao, W. Yang, S. V. Sinogeikin, J. Shu, H.-k. Mao, J. Z. Jiang, Origin of pressure-induced polyamorphism in $ce_{75}al_{25}$ metallic glass, Phys. Rev. Lett. 104 (2010) 105702.

[5] L. Belhadi, F. Decremps, S. Pascarelli, L. Cormier, Y. L. Godec, S. Gorsse, F. Baudelet, C. Marini, G. Garbarino, Polyamorphism in cerium based bulk metallic glasses: Electronic and structural properties under pressure and temperature by x-ray absorption techniques, Appl. Phys. Lett. 103 (11) (2013) 111905.

[6] M. J. Duarte, P. Bruna, E. Pineda, D. Crespo, G. Garbarino, R. Verbeni, K. Zhao, W. H. Wang, A. H. Romero, J. Serrano, Polyamorphic transitions in ce-based metallic glasses by synchrotron radiation, Phys. Rev. B 84 (2011) 224116.

[7] F. Decremps, G. Morard, G. Garbarino, M. Casula, Polyamorphism of a ce-based bulk metallic glass by high-pressure and high-temperature density measurements, Phys. Rev. B 93 (2016) 054209.

[8] M. Wu, J. S. Tse, S. Y. Wang, C. Z. Wang, J. Z. Jiang, Origin of pressure-induced crystallization of ce75al25 metallic glass, Nat. Commun. 6 (2015) 6493.

[9] Q. Zeng, W. L. Mao, H. Sheng, Z. Zeng, Q. Hu, Y. Meng, H. Lou, F. Peng, W. Yang, S. V. Sinogeikin, J.-Z. Jiang, The effect of composition on pressure-induced devitrification in metallic glasses, Appl. Phys. Lett. 102 (17) (2013) 171905.

[10] T. Egami, Atomic size effect of the formability of metallic glasses, J. Non-Cryst. Solids 64 (1984) 113–134.

[11] I. Kantor, V. Prakapenka, A. Kantor, P. Dera, A. Kurnosov, S. Sinogeikin, N. Dubrovinskaia, L. Dubrovinsky, Bx90: A new diamond anvil cell design for x-ray diffraction and optical measurements, Rev. Sci. Instr. 83 (12) (2012) 125102.

[12] T. Irifune, A. Kurio, S. Sakamoto, T. Inoue, H. Sumiya, Ultrahard polycrystalline diamnd from graphite, Nature 421 (2003) 599–600.

[13] N. Ishimatsu, K. Matsumoto, H. Maruyama, N. Kawamura, M. Mizumaki, H. Sumiya, T. Irifune, Glitch-free x-ray absorption spectrum under high pressure obtained using nano-polycrystalline diamond anvils, J. Synchrotron Rad. 19 (5) (2012) 768–772.

[14] O. Mathon, A. Beteva, J. Borrel, D. Bugnazet, S. Gatla, R. Hino, I. Kantor, T. Mairs, M. Munoz, S. Pasternak, F. Perrin, S. Pascarelli, The time-resolved and extreme conditions xas (texas) facility at the european synchrotron radiation facility: the general-purpose exafs bending-magnet beamline bm23, J. Synchrotron Rad. 22 (6) (2015) 1548–1554.

[15] J. Antonowicz, A. Pietnoczka, G. A. Evangelakis, O. Mathon, I. Kantor, S. Pascarelli, A. Kartouzian, T. Shinmei, T. Irifune, Atomic-level mechanism of elastic deformation in the zr-cu metallic glass, Phys. Rev. B 93 (2016) 144115.

[16] F. Birch, Elasticity and constitution of the earth's interior, J. Geophys. Res. 57 (1952) 227–286.

[17] W. H. Wang, Family traits, Nature Mat. 11 (2012) 275–276.